

DOI: 10.1002/((please add manuscript number))

Article type: Communication

Surface Passivation of CIGS Solar Cells using Gallium Oxide

Siddhartha Garud^{1,2}, Nikhil Gampa¹, Thomas G. Allen³, Ratan Kotipalli⁴, Denis Flandre⁴, Maria Batuk⁵, Joke Hadermann⁵, Marc Meuris^{7,8}, Jef Poortmans^{1,6,7}, Arno Smets², Bart Vermang^{7,9}*

S.Garud, N. Gampa, T.G. Allen, Dr. R. Kotipalli, Prof. D. Flandre, Dr. M. Batuk⁵, Prof. J. Hadermann, Dr. M. Meuris, Prof. J. Poortmans, Prof. A.H.M. Smets, Prof. B. Vermang

1 imec- partner in Solliance, 3000, Leuven, Belgium

2 Delft University of Technology, 2628 CD, Delft, The Netherlands

3 Australian National University, Canberra ACT 0200, Australia

4 Université catholique de Louvain, ICTEAM Institute, 1348 Louvain-la-Neuve, Belgium

5 University of Antwerp, Groenenborger Groenenborgerlaan 171, 2020 Antwerp, Belgium

6 Department of Electrical Engineering (ESAT), KU Leuven, 3001, Leuven, Belgium

7 imec division IMOMECE - partner in Solliance, 3590, Hasselt, Belgium

8 Institute for Material Research (IMO) Hasselt University, 3590, Hasselt, Belgium

9 Faculty of engineering technology, Hasselt University, 3590, Hasselt, Belgium

E-mail: bart.vermang@uhasselt.be

Prof. Dr. Bart Vermang

Faculty of engineering technology, Hasselt University, 3590, Hasselt, Belgium

Keywords: CIGS solar cells; surface passivation; gallium oxide; plasma-enhanced atomic layer deposition

This work proposes gallium oxide grown by plasma-enhanced atomic layer deposition, as a surface passivation material at the CdS buffer interface of Cu(In,Ga)Se₂ (CIGS) solar cells. In preliminary experiments, a metal-insulator-semiconductor (MIS) structure is used to compare aluminium oxide, gallium oxide and hafnium oxide as passivation layers at the CIGS-CdS interface. The findings suggest that Gallium oxide on CIGS may show a density of positive charges and qualitatively, the least interface trap density. Subsequent solar cell results with an estimated 0.5 nm passivation layer show an substantial absolute improvement of 56 mV in open-circuit voltage (V_{OC}), 1 mA/cm² in short-circuit current density (J_{SC}), and 2.6 % in overall efficiency as compared to a reference (with the reference showing 8.5 % under AM 1.5G).

Introduction

Cu(In,Ga)(S,Se)₂ solar cells of the chalcopyrite crystal structure have been one of the champions of thin-film technologies, with record laboratory efficiencies reaching 22.6%.^[1] High power conversion efficiencies in crystalline silicon solar cells have been achieved through the invention of complex cell architectures such as PERC (passivated emitter and rear cell). Passivation of the top and rear surfaces and the formation of low resistance contacts cutting through these passivation layers, have been key aspects of high-efficiency silicon solar cell architectures. The 22.6 % record efficiency in CIGS solar cells required a treatment of the top absorber surface with Rubidium fluoride (RbF). Positive effects have also been observed with sodium, potassium and rubidium.^[1, 2] Collectively, they provide new evidence for the role of the CIGS/CdS interface as a limiting factor for high efficiencies. The goal of the work presented in this publication was to introduce a passivation layer between CIGS and CdS and to reduce recombination at this interface in a reproducible manner. An analysis has been presented for the potential of gallium oxide deposited by plasma-enhanced atomic layer deposition, as a passivation layer at the CIGS-CdS interface. A schematic of the cell architecture is shown in **Figure 1 (a)**.

Passivation layers can reduce recombination at a surface and lead to an improvement in open-circuit voltage (V_{oc}) as well as better charge collection (visible in EQE and J_{sc}).^[3, 4, 5] This can be due to a ‘chemical passivation’ which reduces dangling bonds and active interface defects. It may also be due to a ‘field-effect passivation’ which can, based on the polarity of charges in the region, either repel minority charge carriers and reduce recombination or repel majority carriers sufficiently to cause an inversion at the surface.^[6, 7]

Al₂O₃ passivation layers have been recently demonstrated on CIGS solar cells between the CIGS-Mo back contact interface.^[8, 9] At the front interface, CIGS solar cells have often featured buffer layers between the TCO and CIGS absorber. CdS is most commonly used for the band-

alignment at this interface. Another layer such as i-ZnO is used on top of CdS to reduce shunts and maintain electrical homogeneity. However, CdS creates parasitic absorption below 550 nm wavelength of irradiation and Cd is well-known for its toxicity. Koida et al., have recently investigated a-In_{2-2x}Ga_{2x}O₃ as suitable buffer layers with x=0.9 and x=1 giving the most promising results.^[10] The V_{OC} values obtained were comparable to the reference V_{OC} with a i-ZnO/CdS buffer layer, but the FF values were lower. These effects were primarily attributed to a positive conduction band offset which also led to the formation of a secondary barrier and reducing charge collection in forward bias voltages. The height of such a barrier can be reduced by decreasing the thickness of the buffer layer or by increasing the n-type doping in it. Hence, a-GaO_x with thicknesses from 80 nm to 10 nm were attempted with RF sputtering, but incomplete coverage lead to decreased shunt resistance. More recently, Heinemann et al., tested 10 nm to 5 nm layers of a-GaO_x with pulsed laser deposition on CIGS absorbers in superstrate configuration.^[11]

In this aspect, Atomic Layer Deposition (ALD) can provide a unique step forward as it has been proven to be a highly conformal, soft method of deposition for ultra-thin layers.^[12] This is also important due to the rough layer of CIGSe in this work. Furthermore, ultra-thin layers of oxides are required for limiting their contribution to series resistance. Typically, relatively high temperatures are required for ALD growth, such as 150 °C for aluminium oxide and 250 °C for hafnium oxide used in this study. They can introduce unintentional thermal annealing of CIGS absorbers. In this regard, plasma-enhanced atomic layer deposition (PE-ALD) is a particularly advantageous technique since it enables a low deposition temperature (75 °C in this work).^[13]

Experimental Section

Copper, gallium and indium were co-evaporated on soda lime glass/molybdenum substrates with temperatures of around 1350 °C, 1040 °C and 1000 °C respectively, with the substrates heated to 550 °C. The CIGS layer was verified by X-ray fluorescence (XRF) to be 1.7 μm thick. No gallium grading was used and the ratio of copper to gallium and indium (*CGI*) was

approximately 80 % and the ratio of gallium to gallium and indium (*GGI*) was 30 %. All samples were deposited in the same co-evaporation run with very good uniformity.

The substrates were then heated in an annealing step for 15 min at 460 °C with 200 sccm of 10 % H₂Se gas diluted in N₂ to create Cu(In,Ga)Se₂. In order to ensure that the CIGS surface was oxide free for the ALD deposition, all substrates (including the reference) were subjected to an etch by 30 % KCN solution for 1 minute. The samples were then sealed in vacuum until the ALD stage.

GaO_x was deposited via plasma-enhanced ALD at a low temperature of 75 °C and growth rate of 0.07 nm/cycle with Trimethylgallium (TMGa) and oxygen plasma as precursors. Its optical bandgap is expected to be ~4.6 eV as observed by ellipsometry in a previous work.^[13] This is much higher than the CdS bandgap of 2.4-2.5 eV which causes parasitic absorption.^[14] A metal-insulator-semiconductor (MIS) structure such as in **Figure 1 (b)** was created with a gallium oxide layer from 256 cycles of ALD. This created approximately 20 nm of gallium oxide as evidenced in transmission electron microscopy (TEM) (**Figure S1** in supporting information). Completed solar cells were created from ultra-thin layers with namely 4, 8, 32 and 64 cycles leading to estimated maximum thicknesses of 0.3 nm, 0.6 nm, 2.3 nm, and 4.5 nm of gallium oxide. All the plasma-enhanced atomic layer depositions were carried out at the Australian National University in Canberra. In other test samples, aluminium oxide was deposited via thermal ALD with trimethylaluminium (TMA) (pulse time: 0.016 ms, purge time: 40 s) and water (pulse time: 0.03 ms, purge time: 20 s) as precursors at a temperature of 150 °C. A linear growth rate of 0.12 nm/cycle was achieved. Hafnium oxide was similarly deposited via thermal ALD with Tetrakis(ethylmethylamino)hafnium (TEMAH) (pulse time: 0.1 ms, purge time: 35 s) and water (pulse time: 0.01 ms, purge time: 30 s) as precursors at a temperature of 250 °C leading to a linear growth rate of 0.11 nm/cycle.

The substrates were then subjected to chemical-bath deposition of CdS (~ 50 nm), sputtering of 100 nm intrinsic ZnO and 400 nm Al-doped ZnO (total sheet resistance of 50 ohm) and e-beam

deposition of Ni/Al/Ni front grids. Two to five cells of 0.5 cm² area were mechanically scribed on each substrate.

Capacitance-voltage measurements

An MIS structure was first created to assess aluminium oxide (29 nm), gallium oxide (20 nm) and hafnium oxide (20 nm) as passivation layers grown by ALD. A schematic of the structure is shown in **Figure 1 (b)**. Capacitance-voltage measurements were made in order to study the density of charges in the oxide layers and the interface trap density. The former was calculated from the flat-band condition. In order to maintain voltage stability of measurements, unanalysed devices were measured in a single sweep under the same temperature and dark conditions. This would exclude any voltage dependent-hysteresis. The normalized capacitance voltage measurements of the three devices at 100 kHz are shown in **Figure 2**. They indicate flat-band voltages as summarized in **Table 1**.

The flat-band voltages can be attributed to a density of charges present in the oxide, which can be calculated with the following equation: ^[15]

$$Q_f = C_{ox} \frac{(\phi_{ms} - V_{fb})}{e} \quad (1)$$

Here Q_{eff} is the effective charge density in cm⁻², C_{ox} is the oxide capacitance in F/cm², e is elementary charge in coulombs and ϕ_{ms} is the work-function difference between the Al metal contact and the CIGS semiconductor. C_{ox} was calculated using the oxide thicknesses mentioned earlier (verified with TEM in the case of GaO_x) and estimated dielectric constants of 7.6 for AlO_x ^[16], 9.2 for GaO_x ^[17] and 18.7 for HfO_x. ^[18] It can be noted here that while the dielectric constant of these oxides can slightly vary based on the substrate layer and deposition process, they would not change the order of magnitude of the effective charge density (Q_{eff}). The work function difference (ϕ_{ms}) was calculated using the following equations: ^[15]

$$\phi_{ms} = \phi_m - \left(\chi + \frac{E_g}{2} + \phi_{fp} \right) \quad (2)$$

$$\phi_{fp} = V_t \ln \frac{N_a}{n_i} \quad (3)$$

$$n_i = \sqrt{N_C N_V e^{-E_g/kT}} \quad (4)$$

Here ϕ_m is the work-function of metal aluminium with an average of 4.17 eV. ^[19] E_g is the bandgap of CIGS (1.15 eV), and χ is electron affinity which was taken to be in the range of 3.9-4.5 eV. ^[20] ϕ_{fp} was calculated for an acceptor concentration of $N_a = 5 \times 10^{15} \text{ cm}^{-3}$ and intrinsic carrier concentration (n_i) of $7 \times 10^8 \text{ cm}^{-3}$. n_i was calculated from conduction-band density of states ($N_C = 7 \times 10^{17} \text{ cm}^{-3}$) and valence-band density of states ($N_V = 1.5 \times 10^{19} \text{ cm}^{-3}$) and k being the Boltzmann constant. ^[7, 20]

For the range of CIGS electron affinity (χ) of 3.9-4.5 eV, charge densities (Q_{eff}) were calculated as shown in **Table 1**. In the case of GaO_x , Q_{eff} is positive with a values in the range of $1.4 \times 10^{12} \text{ cm}^{-2}$ to $5.8 \times 10^{11} \text{ cm}^{-2}$ in case of $\chi = 3.9-4.4 \text{ eV}$ or weakly negative if CIGS is assumed to have a higher electron affinity. Since the doping levels in CIGSe material of these experiments are comparatively low (10^{15} cm^{-3}), an oxide with positive charge could form a depletion layer and improve charge collection at the front CIGS-CdS interface. This effect has been theoretically studied by Sozzi et al., ^[6] and Bercegol et al. ^[7]. In contrast, AlO_x shows high negative charge densities between -2×10^{11} to -1×10^{12} which is consistent with previous observations. ^[9]

A quantitative assessment of the D_{it} at the oxide-semiconductor interface has not been yet achieved due to the difficulty in conductance measurements at room temperature on these devices. (i.e. no parallel conductance peaks were detected). Nevertheless, we assume that low temperature measurements on these devices could provide more insights on the defect-state densities and distributions within the bandgap, such as in a previous work with AlO_x ^[9].

In order to provide at least a qualitative assessment of D_{it} , the slope of the graphs in **Figure 2**. have been highlighted as dashed lines. According to the Terman method, $C-V$ curves of a MIS capacitor can be interpreted as surface potential (ϕ_s) vs gate voltage curves, which contain information on the interface trap density. Surface potential fluctuations due to presence of

interface states will therefore induce a spread in the C - V curves (especially in the depletion regime) as noticed in **Figure 2**. Gallium oxide clearly shows the most negative slope or in other words, the least D_{it} among these three samples.

With these encouraging results, solar cells were processed with varying thicknesses of gallium oxide deposited by the low temperature (75 °C) plasma-enhanced ALD on the CIGSe layer. The actual thickness of the gallium oxide layers on CIGSe after deposition and after CdS chemical bath deposition, are as yet, not verifiable as thicknesses less than 1 nm on such a rough CIGS surface were difficult to detect even with TEM. Nevertheless, all the solar cells were processed together in a stable process line and some differences in photoluminescence and electrical characterization are clearly visible and discussed in the following sections. Minimum temperatures of 127 °C -300 °C are typically required to observe significant thermal annealing effects and hence, we expect 75 °C to not have any such impact. [21, 22, 23, 24]

Photoluminescence

The passivation layers have a significant effect on photoluminescence (PL) and carrier lifetime. In **Figure 3**, PL measurements show that all cells were equivalent when the absorber layers were created (dashed lines). In the stage after a KCN etch, after the deposition of gallium oxide and before CdS deposition, no significant differences are visible except for the sample with 4 cycles of ALD (dotted lines). The formation of a p-n junction by the deposition of CdS and TCO seems to be necessary to see a higher photoluminescence response and differences between cells (solid lines). This is visible in the reference cell. However, a further increase in response was recorded for the cells with passivation layers starting from 4 cycles to 64 cycles. The highest response was recorded for the cell with 8 cycles of ALD.

An increase in carrier lifetime was also observed with 8 ALD cycles; up to 9 ns as compared to 3 ns in the reference and other samples (**Figure 4**). A 2nd order exponential fitting was used for the time-resolved photoluminescence (TRPL) with the equation $I_{PL}(t) = C_1 e^{-t/\tau_1} + C_2 e^{-t/\tau_2}$

(**Figure S2** and **Table S1** in the supporting information). The value of τ_2 has been used as an indication of charge carrier lifetime.

These improvements indicate that the GaO_x layers are able to passivate charge carrier traps on the top surface which otherwise act as recombination centers.

Electrical performance parameters

Next, the electrical parameters were characterized. The reduction in recombination is visible in V_{OC} as shown in **Figure 5**. It shows a clear increasing trend up to an optimum 8 cycles of ALD. The box plots were created with values from 2-5 cells in each case. J - V curves of the best cells from each device are shown in **Figure 6**. A one-diode model was used for analysis based on the methods by Hegedus et al., and the results are shown in the inset of **Figure 6**.^[25] The calculated dark saturation current (J_0) correlates well with the V_{OC} , which are indicators of the total recombination in the cells. In the case of the cell with 8 cycles of ALD, good shunt resistance is also observed as a contributor to V_{OC} . The series resistance was higher when 32 cycles of ALD were used. In the sample with 64 cycles of ALD, shunting was observed which may have been caused due to unavoidable physical damage to the sample. This data is nevertheless, included for completeness as its behavior in forward bias is similar to those of the other cells (**Figure 6**). With all these factors combined, an increasing trend in cell efficiency is observed with up to 8 cycles of ALD (**Figure 5**) with an absolute increase of 2.6 % in efficiency, 1.04 mA/cm² in J_{SC} , 56.3 mV in V_{OC} and 8.22 % in FF as compared to the reference. One reason for the improved J_{SC} was observed in the EQE (**Figure 7**) wherein better response was observed primarily at shorter wavelengths (500 - 800 nm).

Summary

An effective passivation layer can significantly reduce surface recombination and also increase reproducibility in solar cells via a reliable processing step. In addition, plasma-enhanced ALD has showcased a low-temperature of deposition (75 °C) which avoids undesirable annealing

effects. ALD growth is currently the most suitable choice for thin-layers of conformal growth on even rough surfaces of photovoltaic materials.

This work presents gallium oxide deposited via Plasma-enhanced ALD as a potential passivation layer for CIGSe. Capacitance-voltage measurements on MIS structures have shown gallium oxide to likely have positive charge densities around 1.4×10^{12} to $5.8 \times 10^{11} \text{ cm}^{-2}$ and low D_{it} as compared to aluminium oxide and hafnium oxide. Improved photoluminescence response was observed with the inclusion of gallium oxide in the cell architecture.

In the case of preliminary solar cell results, it is as yet unclear if ultra-thin layers (<2 nm) can survive the chemical bath deposition of CdS. Nevertheless, since gallium oxide showcased passivation effects in the C - V and photoluminescence studies, solar cells were fabricated along with a reference in a stable process line. The electrical characterization of these cells did indeed show an absolute increase of 2.6 % in efficiency originating from a substantial increase of 56.3 mV in V_{OC} , 1.04 mA/cm² in J_{SC} , and 8.22 % in FF with a gallium oxide layer as compared to the reference. Therefore as an outlook, future experiments can focus on alternative buffer layers or deposition techniques, point contact openings through thick gallium oxide layers (such as those simulated by Sozzi et al.,^[6] and Bercegol et al.,^[7]) and also low-temperature conductance measurements on MIS structures to quantify D_{it} .

Acknowledgements

The work published in this paper was supported by the European Research Council (ERC) under the Union's Horizon 2020 research and innovation programme (grant agreement No 715027). The authors would also like to thank Dr. Marcel Simor (Solliance) for the CIGS layer fabrication and Prof. Johan Lauwaert (Universtiy of Ghent) for his guidance on DLTS measurements.

Received: ((will be filled in by the editorial staff))

Revised: ((will be filled in by the editorial staff))

Published online: ((will be filled in by the editorial staff))

References

- [1] P. Jackson, R. Wuerz, D. Hariskos, E. Lotter, W. Witte and M. Powalla, *PSS (RRL)*, **2016**, vol. 10, no. 8, p. 583–586.
- [2] P. Reinhard, B. Bissig, F. Pianezzi, E. Avancini, H. Hagendorfer, D. Keller, P. Fuchs, M. Döbeli, C. Vigo, P. Crivelli, S. Nishiwaki, S. Buecheler and A. N. Tiwari, *Chemistry of Materials*, **2015**, vol. 27, pp. 5755-5764.
- [3] M. Green, *Solar Energy Materials and Solar Cells*, 2015, vol. 143, pp. 190-197.
- [4] B. Vermang, T. J. Wätjen, V. Fjällström, F. Rostvall, M. Edoff, R. Kotipalli, F. Henry and D. Flandre, *Progress in Photovoltaics: Research and Applications*, **2014**, vol. 22, no. 10, pp. 1023-1029.
- [5] M. J. J. V. B. & H. C. Edoff, *Photovoltaic Specialists Conference (PVSC), 2016 IEEE 43rd*, **2016**, pp. 3527-3530.
- [6] G. Sozzi, S. D. Napoli, R. Menozzi, B. Bissig, S. Buecheler and A. N. Tiwari, *Solar Energy Materials & Solar Cells*, **2017**, vol. 165, pp. 94-102
- [7] A. Bercegol, B. Chacko, R. Klenk, I. Lauermann, M. C. Lux-Steiner and M. Leiro, *Journal of Applied Physics*, **2016**, vol. 119, no. 15, pp..
- [8] B. Vermang, V. Fjällström, X. Gao and M. Edoff, *IEEE Journal of Photovoltaics*, **2014**, vol. 4, no. 1, pp. 486-492..
- [9] R. Kotipalli, B. Vermang, J. Joel, R. Rajkumar and M. Edoff and D. Flandre, *AIP advances*, **2015**, vol. 5, no. 107101, pp. 1-6.
- [10] T. Koida, Y. Kamikawa-Shimizu, A. Yamada, H. Shibata and S. Niki, *IEEE Journal of photovoltaics*, **2015**, vol. 5, no. 3, pp. 956-961
- [11] M. Heinemann, M. F. A. M. van Hest, M. Contreras, J. D. Perkins, A. Zakutayev, C. Kaufmann, T. Unold, D. S. Ginley and J. J. Berry, *Physica Status Solidi (a)*, **2017**, vol. 214, no. 5, pp. 1-6.
- [12] H. B. Profijt, S. E. Potts, M. C. M. Van de Sanden and W. M. M. & Kessels, *Journal of Vacuum Science & Technology A: Vacuum, Surfaces, and Films*, **2011**, vol. 29, no. 5, p. 050801
- [13] T. G. Allen, M. Ernst, C. Samundsett and A. Cuevas, *IEEE Journal of Photovoltaics*, **2015** vol. 5, no. 6, pp. 1586-1590.
- [14] J. Dona and J. Herrero, *J. Electrochem. Soc.*, **1997**, vol. 144, pp. 4081-4091.
- [15] D. Schroder, *Semiconductor material and device characterization*, Hoboken: John Wiley & Sons Inc, **2006**.
- [16] M. Groner, J. Elam, F. Fabreguette and S. George, *Thin Solid Films*, **2002**, vol. 413, no. 1-2, pp. 186-197.
- [17] D.W. Choi, K.B. Chung and J.S. Park, *Thin Solid Films*, **2013**, vol. 546, pp. 31-34.
- [18] J. Robertson, *Journal of Applied Physics*, **2008**, vol. 104, no. 12, p. 124111.
- [19] W. M. Haynes, *CRC handbook of chemistry and physics*, Boca raton: CRC press, **2014**.
- [20] C. Frisk, C. Platzer-Björkman, J. Olsson, P. Szaniawski, J. T. Wätjen, V. Fjällström, P. Salomé and M. Edoff, *Journal of Physics D: Applied Physics*, **2014**, vol. 47, no. 48, pp. 1-12.
- [21] E. Moons, D. Gal, J. Beier, G. Hodes, D. Cahen, L. Kronik, B. L., B. Mishori, Y. Shapira, D. Hariskos and H. Schock, *Solar energy materials and solar cells*, **1996**, vol. 43, no. 1, pp. 73-78.
- [22] Y.-D. Chung, D.-H. Cho, N.-M. Park, K.-S. Lee and J. Kim, *Current Applied Physics*, **2011**, vol. 11, no. 1, pp. S65-S67.

- [23] D. S. Chen, J. Yang, Z. B. Yang, F. Xu, H. W. Du and Z. Q. and Ma, *Materials Research Bulletin*, **2014**, vol. 54, pp. 48-53,.
- [24] T. Sakurai, N. Ishida, S. Ishizuka, M. M. Islam, A. Kasai, K. Matsubara, K. Sakurai, A. Yamada, K. Akimoto and S. and Niki, *Thin Solid Films*, **2008**, vol. 516, no. 20, pp. 7036-7040.
- [25] S. S. Hegedus and W. N. Shafarman, *Progress in photovoltaics: Research and applications*, **2004**, vol. 12, pp. 155-176.

Figure 1. Schematics of the solar cell architecture with the gallium oxide passivation layer shown between CIGS and CdS (a) and Metal-insulator-semiconductor structure used for capacitance-voltage measurements (b) (not to scale)

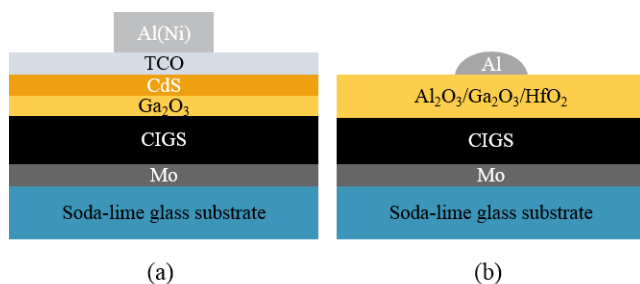


Figure 2. Normalized capacitance-voltage curves at 100 kHz for MIS structures with AlO_x , GaO_x and HfO_2

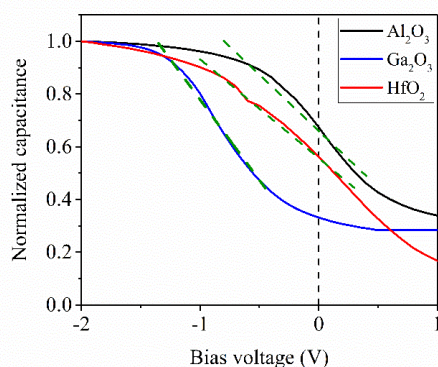


Figure 3. Photoluminescence measurements show the similarity between as-deposited absorbers (dashed lines) and differences in the completed cells (solid lines) possibly arising from GaO_x deposition.

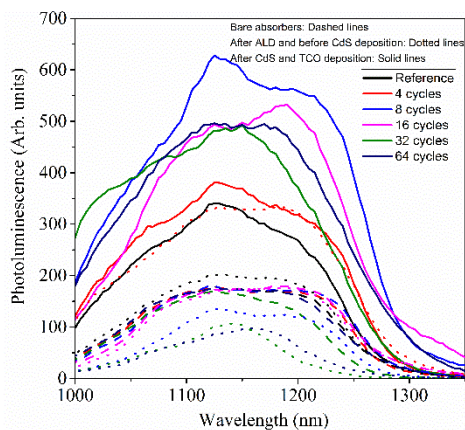


Figure 4. Higher charge carrier lifetime was observed with 8 cycles of ALD as compared to the reference and other samples.

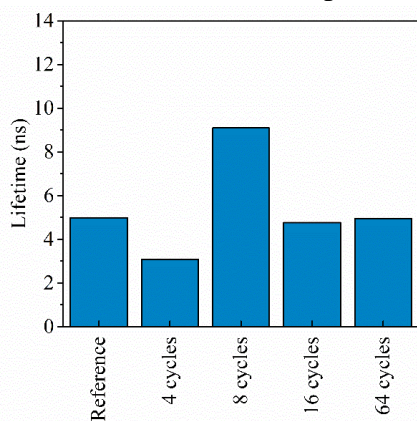


Figure 5. Electrical parameters of completed solar cells (2-5 cells in each case) show optimal values with 8 cycles of ALD

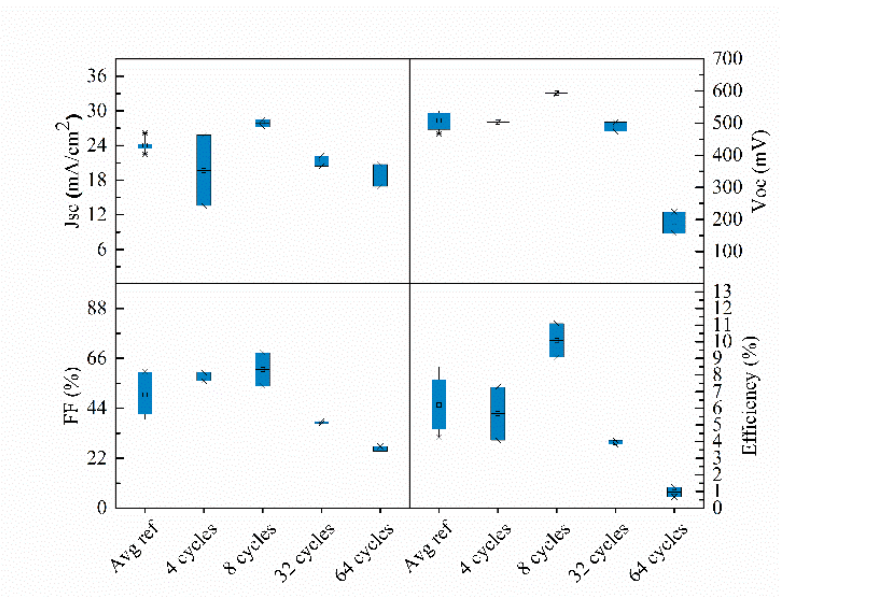


Figure 6. *J-V* curves of the best cells from each device show the reduction in recombination and increased shunt resistance with 8 cycles of ALD as compared to the reference. An increase in series resistance is visible with 32 cycles of ALD. A one-diode model was used for analysis according to the methods by Hegedus et al. [21]

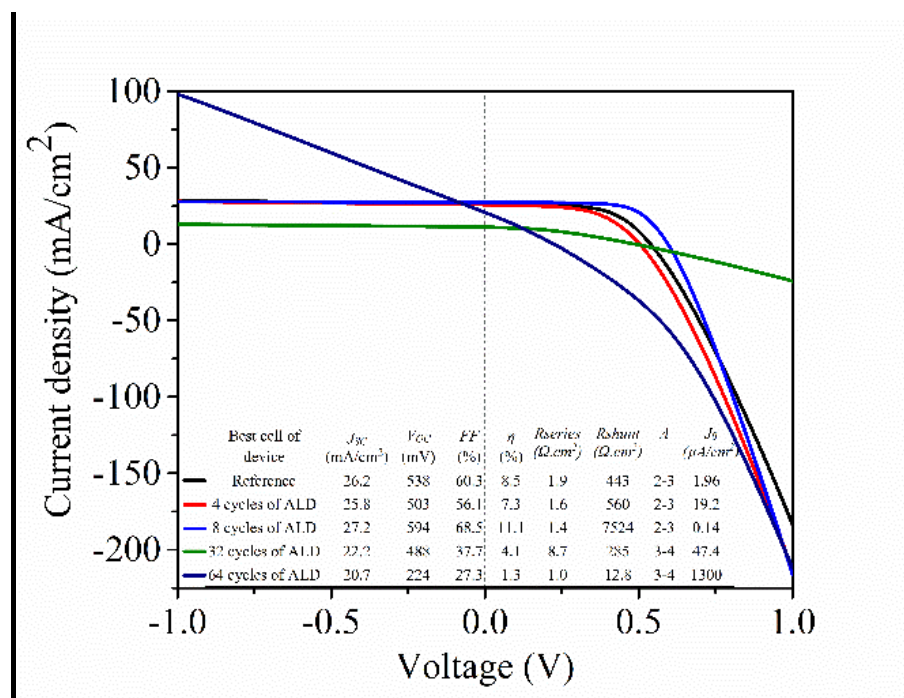


Figure 7. EQE of the cell with 8 cycles of ALD was observed to be better than that of the reference cell at the shorter wavelengths (500 - 800 nm).

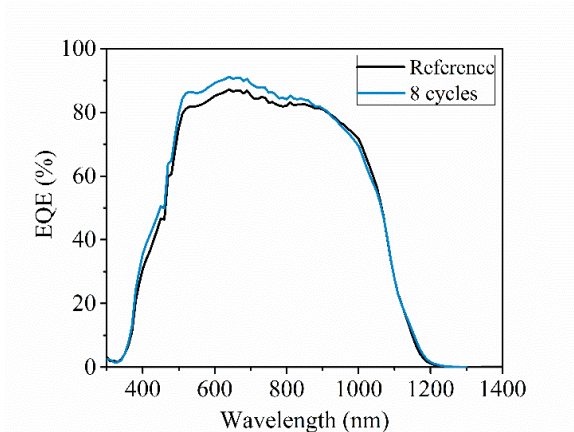


Table 1. Flat-band voltage calculated from C-V measurement

Oxide layer	Flat-band Voltage (V_{fb}) (V)	Oxide capacitance (C_{ox}) (F/cm ²)	Charge density (Q_{eff})(cm ⁻²) with $\chi_{CIGS} = 3.9$ eV	Charge density (Q_{eff})(cm ⁻²) with $\chi_{CIGS} = 4.2$ eV	Charge density (Q_{eff})(cm ⁻²) with $\chi_{CIGS} = 4.5$ eV
AlO _x	-0.5	2.7×10^{-7}	-2.0×10^{11}	-6.4×10^{11}	-1.1×10^{12}
GaO _x	-1.2	4.1×10^{-7}	1.4×10^{12}	5.8×10^{11}	-1.8×10^{11}
HfO _x	-1	8.3×10^{-7}	1.3×10^{12}	-2.1×10^{11}	-1.76×10^{12}

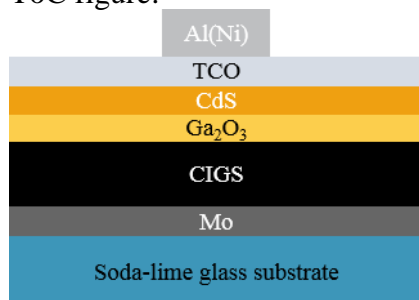
Table of contents entry: This work proposes gallium oxide as a surface passivation layer on the photovoltaic material in Cu(In,Ga)Se₂ (CIGS) solar cells. A metal-insulator-semiconductor (MIS) structure is used to compare aluminium oxide, gallium oxide and hafnium oxide for this purpose. Solar cells fabricated with gallium oxide deposited between the CIGS and CdS buffer layer interface, show better performance than reference cells.

Keywords: CIGS solar cells; surface passivation; gallium oxide; plasma-enhanced atomic layer deposition

*S.Garud, N. Gampa, T. Allen, Dr. R. Kotipalli, Prof. D. Flandre, Dr. M. Batuk⁵, Prof. J. Hadermann, Dr. M. Meuris, Prof. J. Poortmans, Prof. A.H.M. Smets, Prof. B. Vermang**

Surface passivation of CIGS solar cells using gallium oxide

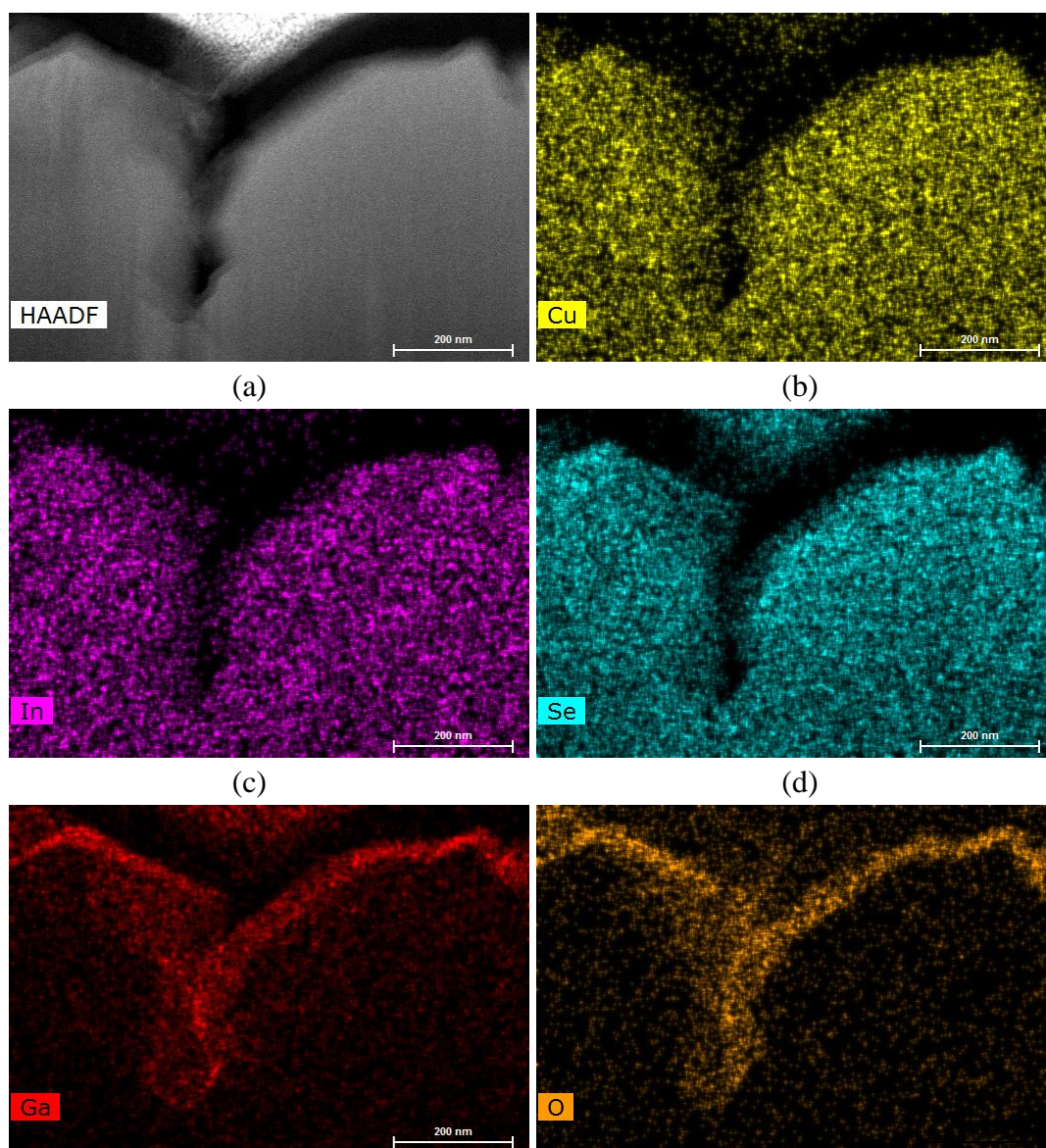
ToC figure:



Copyright WILEY-VCH Verlag GmbH & Co. KGaA, 69469 Weinheim, Germany, 2016.

Supporting Information

Figure S1 Overview image from high-angle annular dark-field imaging- scanning transmission electron microscope (HAADF-STEM) (a), individual elemental maps (in counts) (b-f), and mixed Cu/In/Ga/Se map (g). Gallium oxide deposited by plasma-enhanced atomic layer deposition on a rough CIGS surface shows highly conformal growth of 20 nm thickness even in cracks.



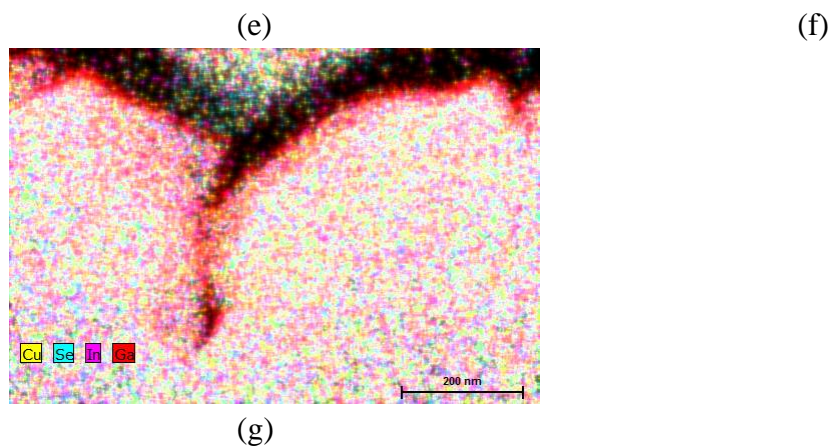


Figure S2 The time-resolved photoluminescence (TRPL) of each cell shown here was fitted with a 2nd order exponential equation (Please see **Table S1**).

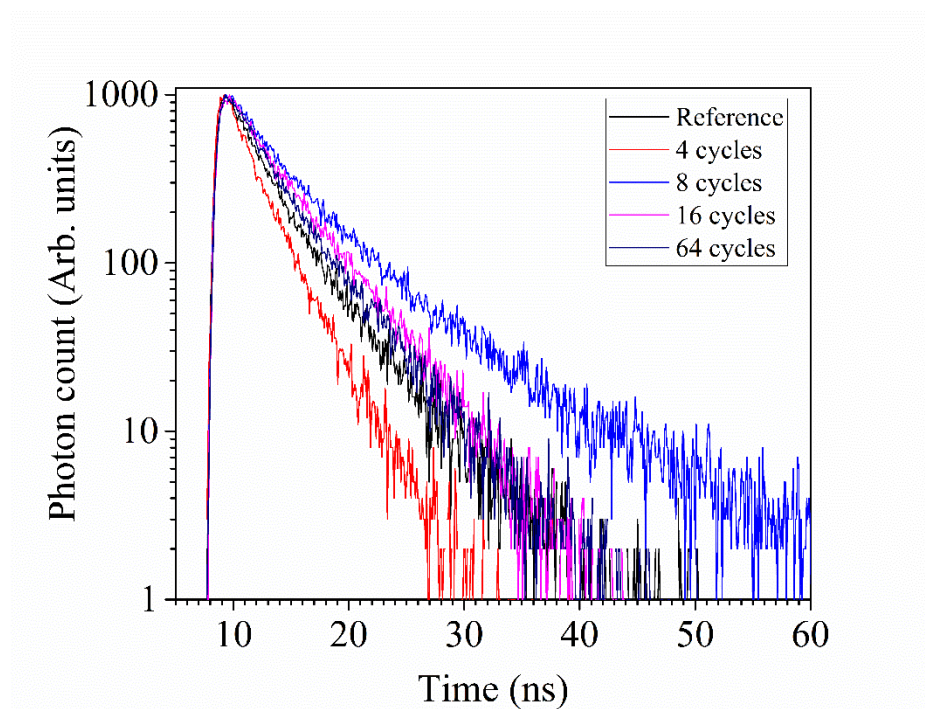


Table S1 A 2nd order exponential fitting was used for the time-resolved photoluminescence (TRPL) with the equation $I_{PL}(t) = C_1 e^{-t/\tau_1} + C_2 e^{-t/\tau_2}$. The value of τ_2 has been shown as an indication of charge carrier lifetime in **Figure 4**.

Sample	CHI	τ_1	τ_2
Reference	1.05	2.3	5
4 cycles	0.9	1.2	3.1
8 cycles	1.2	3.4	9.1
16 cycles	1.2	1.3	4.8
64 cycles	1.1	2.3	4.9

